View metadata, citation and similar papers at core.ac.uk

brought to you by CORE

provided by NASA Technical Reports Server

DEC 29 1946

ACR No. L4G28

NATIONAL ADVISORY COMMITTEE FOR AERONAUTICS

# WARTIME REPORT

ORIGINALLY ISSUED

July 1944 as
Advance Confidential Report L4G28

## ESTIMATION OF PRESSURE DISTRIBUTIONS AT SUBCRITICAL SPEEDS FOR TURRETS LOCATED ON A WING

By Virgil S. Ritchie and Everett J. Daniels

Langley Memorial Aeronautical Laboratory
Langley Field, Va.

NACA

WASHINGTON

N A C A LIBRARY
LANGLEY MEMORIAL AERONAUTICAL
LABORATORY
Langley Field, Va.

NACA WARTIME REPORTS are reprints of papers originally issued to provide rapid distribution of advance research results to an authorized group requiring them for the war effort. They were previously held under a security status but are now unclassified. Some of these reports were not technically edited. All have been reproduced without change in order to expedite general distribution.

NASA Technical Library
3 1176 01403 3741

NACA ACR No. L4G28

NATIONAL ADVISORY COMMITTEE FOR AERONAUTICS

ADVANCE CONFIDENTIAL REPORT

# ESTIMATION OF PRESSURE DISTRIBUTIONS AT SUBCRITICAL SPEEDS FOR TURRETS LOCATED ON A WING

By Virgil S. Ritchie and Everett J. Daniels

## SUMMARY

Current methods that take into account interference and compressibility effects have been used to estimate pressures over and near turrets located on a wing in regions of high interference velocities.

Graphical comparisons of measured pressures, available from wind-tunnel tests, and estimated pressures are presented for angles of attack of $0^\circ$, $1^\circ$, and $4^\circ$ at Mach numbers up to 0.650. The agreement between measured and estimated pressures indicated that present methods are adequate for predicting approximate critical speeds and for estimating loads at subcritical speeds with sufficient accuracy for design purposes. The methods used in this paper were not applicable at speeds much higher than the critical.

## INTRODUCTION

The investigation reported in the present paper was made in order to check the applicability of current methods, suggested in reference 1, to pressure estimations involving large interference effects. Prior to this investigation, successful predictions of pressure distributions for gun turrets and similar shapes were for the most part limited to protuberances located on fuselages, where the interference was usually negligible. The applicability of current methods to estimations involving high interference velocities was uncertain because of insufficient experimental data with which to compare estimates. Recent tests of a turret model in the NACA 8-foot high-speed tunnel (unpublished), however, provided the experimental data necessary for investigating the accuracy of predictions for turret-like

protuberances located in regions of high interference velocities. The purpose of the present paper is to apply current methods, including interference and compressibility effects, to the estimation of pressure distributions for this turret, for which measured data are available, and to compare the estimates with measurements.

Present theory, which does not hold at speeds much higher than the critical, limited the Mach number range for the estimations. Practical comparisons were made at a subcritical speed (Mach number $M = 0.275$) and at the approximate critical speed ($M = 0.500$); a few comparisons were made at a supercritical speed ($M = 0.650$) to show the inadequacy of the methods used at subcritical speeds when applied in the supercritical range. Angles of attack for which the estimations were made ($0^\circ$, $1^\circ$, and $4^\circ$) were determined largely by the range of experimental values available for comparison.

This and similar applications of current estimating methods are valuable because they indicate that predictions may be substituted for the more expensive wind-tunnel tests of turret-like protuberances when approximate critical speeds and loads at subcritical speeds are desired.

## SYMBOLS

| | |
|---|---|
| $P$ | pressure coefficient |
| $V$ | velocity |
| $V/V_o$ | velocity ratio; total unless indicated otherwise by subscript |
| $\Delta V$ | velocity increment |
| $\Delta V/V_o$ | velocity-increment ratio, induced velocity, or interference velocity |
| $M$ | Mach number |
| $\alpha$ | wing angle of attack, degrees |

[redacted]

$\gamma$ ratio of specific heat at constant pressure to specific heat at constant volume for air $(c_p/c_v)$

Subscripts:

| | |
|---|---|
| abs | absolute |
| cr | critical; at speed of sound |
| i | incompressible |
| max | maximum value |
| min | minimum value |
| o | free stream |
| t | turret |
| w | wing |
| 2D | two-dimensional flow |
| 3D | three-dimensional flow |

## DESCRIPTION OF TURRET SHAPES

The turret installation, for which experimental data are available and for which estimates are made in this investigation, is shown in figure 1. Identical turret domes are mounted on both upper and lower surfaces of a 24-inch-chord section of a symmetrical airfoil approximately 19 percent thick. Both turrets are rotated -3.19° with respect to the wing chord line and the lower turret is located slightly nearer the wing leading edge than is the upper turret. These factors of turret angle and location necessitate different filleting between the dome skirts and the wing surfaces. If the flow to which the turrets are subjected is considered parallel to the surfaces of the wing, the ordinates for the effective turret shapes should consequently be measured from the wing surface to include fillet thickness and thus effectively change the shapes of the turrets by different amounts.

[redacted]

Figure 2 shows a comparison of the actual shapes of the turrets as installed on the wing, and the effective shapes with the wing surface reduced to a straight line.

## PROCEDURE

Pressure distributions for the turrets were estimated by the methods of reference 1. The boundary layer over the streamline shape of the turret was considered negligible and the flow was assumed to follow the surface without separation. The estimations were limited to the three regions considered most important over and near the turret in its normal position. In figure 3, these regions are identified as: line 1, chordwise over the top of and extended in front of the turret central meridian; line 2, over the rim or base of the turret; line 3, spanwise over the top of and extended from the side of the turret at the point of maximum thickness.

For computational purposes, the effective turret shapes (fig. 2(b)) were resolved into simple geometrical forms that could be expressed by analytic equations. Velocity distributions over the turrets were calculated from these equations and interference effects were included by adding calculated wing induced velocities to the turret velocities; velocities over the wing surface near the turret were corrected for interference by adding induced velocities due to the turrets. Total velocities including interference were then converted into pressure coefficients and compressibility adjustments were applied.

## ESTIMATION OF PRESSURES OVER TURRET

Chordwise central meridian (line 1, fig. 3).- The slope method (reference 1) was used to calculate approximate two-dimensional velocity-increment ratios for potential flow over simple geometrical shapes best fitting the turret profile. By this method, the velocity distribution is a function of the slope with accuracy greatest in regions of little slope (near turret maximum thickness) and with error most likely in regions of steep slope (near turret leading and trailing edges).

[redacted]

The shapes best representing the turret profile consisted of a circular arc fitting the forward portion of the profile and a parabolic arc fitting the rearward portion with the slopes of the two arcs continuous at the point of juncture near the turret maximum thickness. (See fig. 2(b).) The origin for equations representing these shapes is on the axis of the turret immediately below the point of juncture. The velocity-increment ratio is expressed as the sum of two integrals corresponding to the arcs constituting the turret profile in the following equation:

$$\frac{\Delta V}{V_o} = \frac{1}{\pi}\int_{L.E.}^{O} \frac{dy_1/dx}{x' - x}\,dx + \frac{1}{\pi}\int_{O}^{T.E.} \frac{dy_2/dx}{x' - x}\,dx \qquad (1)$$

where the slopes $dy_1/dx$ and $dy_2/dx$ are algebraic functions of the abscissa $x$ and $\Delta V/V_o$ is a function of the abscissa of any point at which velocities are desired $x'$. In the equation the first integral corresponds to the circular arc and its limits are from the turret leading edge L.E. to the origin or point of juncture of the arcs O. The second integral corresponds to the parabolic arc and its limits are from the origin O to the turret trailing edge T.E.

Velocity ratios were obtained from the calculated velocity-increment ratios by the relation

$$\frac{V}{V_o} = \frac{\Delta V}{V_o} + 1 \qquad (2)$$

and are shown as solid lines in figure 4. These calculated approximate two-dimensional velocity ratios were corrected to the three-dimensional ratios $(V/V_o)_{3D}$ for the turret by means of an empirical correction factor determined from available data for a similar shape (turret B, reference 2). This factor, expressed as a ratio of experimental $(V/V_o)_{3D}$ to calculated $(V/V_o)_{2D}$,

[redacted]

is shown as long-dash lines in figure 4. The magnitude of this correction factor was checked for the forward portion of the turret by comparing it with ratios of calculated velocities for flow over the elliptical section of an equivalent oblate spheroid to calculated two-dimensional velocities about the corresponding elliptic cylinder. The values of $(V/V_o)_{3D}$ obtained by multiplying the calculated values of $(V/V_o)_{2D}$ by the correction factor at corresponding distances from the turret leading edge are shown as short-dash lines in figure 4.

Wing velocity distributions for incompressible flow were calculated by the method of reference 3 for angles of attack of $0^\circ$, $1^\circ$, and $4^\circ$. Velocity distributions calculated by this method are usually reasonably accurate but experimental values would probably be preferable. Figure 5 shows the calculated velocities, expressed as interference velocities or velocity-increment ratios, for the wing alone at $M = 0$.

Total velocities over the turret with wing interference were obtained by adding the estimated velocity ratios for the turret shape alone (fig. 4) to the calculated wing velocity-increment ratios (fig. 5); thus

$$\frac{V}{V_o} = \left(\frac{V}{V_o}\right)_t + \left(\frac{\Delta V}{V_o}\right)_w$$

The resulting total velocities are shown in figure 6.

Pressure coefficients corresponding to the total velocities were obtained from the low-speed relation

$$P_i = 1 - \left(\frac{V}{V_o}\right)^2 \tag{3}$$

and these values were adjusted for Mach number by the von Kármán relation (reference 4)

$$P = \frac{P_i}{\sqrt{1 - M^2} + \dfrac{M^2}{2\left(1 + \sqrt{1 - M^2}\right)} P_i} \tag{4}$$

The estimated peak negative pressure coefficients against Mach number are shown in figure 7 with the measured values. The intersection of these curves with the curve for critical pressure coefficient $P_{cr}$ (the curve of pressure coefficient corresponding to the local speed of sound) indicates a critical Mach number of about 0.500 for either the upper or lower turret with wing interference; this value was taken as the limiting Mach number for application of the pressure-distribution estimations, since the methods used in the present paper do not hold at speeds much higher than the critical.

Figures 8, 9, and 10 show pressure-distribution estimates for the turrets with wing interference at angles of attack of $0^\circ$, $1^\circ$, and $4^\circ$, respectively. Measured values are shown for comparison. The measured values shown in figure 8 were obtained from cross plots of measured pressure coefficients against angle of attack.

Rim (line 2, fig. 3).- The forward portion of the upper turret can be approximated by an equivalent oblate spheroid as shown in figure 11.

Motion of the oblate spheroid perpendicular to its polar axis corresponds to that of the turret. The potential is given in terms of the semielliptic coordinates $\mu$, $\zeta$, and $\omega$ in reference 5. The velocity relative to the body can be obtained for any point from

$$\left(\frac{V}{V_o}\right)^2 = \left(\frac{B\zeta}{\zeta^2 + 1} - B \cot^{-1}\zeta + 1\right)^2 + 4B\frac{1 - \mu^2}{\zeta^2 + 1}\frac{\cos^2\omega}{\zeta^2 + \mu^2}\left(B - B\zeta \cot^{-1}\zeta + \zeta\right) \quad (5)$$

where

$$B = -\frac{1}{\frac{\zeta_o^2 + 2}{\zeta_o(\zeta_o^2 + 1)} - \cot^{-1}\zeta_o}$$

[redacted]

$$\zeta_o = \frac{b}{a} \frac{1}{\sqrt{1 - \left(\frac{b}{a}\right)^2}} \tag{6}$$

a is the semimajor axis, and b is the semiminor axis for the elliptical section of the oblate spheroid. For points on the surface of the spheroid, $\zeta = \zeta_o$.

At the surface around the rim (line 2), $\mu = 0$, $\zeta = \zeta_o$, equation (5) reduces to

$$\left(\frac{V}{V_o}\right)_{rim} = L \sin \omega \tag{7}$$

where

$$L = \frac{2}{\zeta_o^2 + 2 - \zeta_o\left(\zeta_o^2 + 1\right) \cot^{-1}\zeta_o}$$

and the distance from the leading edge x is given by

$$x = a(1 - \cos \omega)$$

Over the top (line 1), $\omega = 0$ and

$$\left(\frac{V}{V_o}\right)_{top} = L\mu\left(\frac{\zeta_o^2 + 1}{\zeta_o^2 + \mu^2}\right)^{1/2} \tag{8}$$

where

$$x = a\left(1 - \sqrt{1 - \mu^2}\right)$$

The velocity distribution around the rim of the forward portion of the turret could be approximated by the velocity distribution about the rim of the oblate spheroid (equation (7)) as shown by the short-dash lines

in figure 12. Experimental data indicate, however, that the shape of the velocity distribution around the rim of such a regular body bears a close resemblance to that over the central meridian in the direction of motion. (See solid line in fig. 12.) At corresponding positions along the oblate spheroid and along the turret length in the x-direction, the ratio of velocities at the rim to those at the top of the oblate spheroid (see short-dash and long-dash lines in fig. 12) were therefore assumed to hold for the turret also. From this ratio (calculated for the oblate spheroid) and the velocities previously calculated by the slope method for the chordwise central meridian of the turret (see solid line in fig. 12.), the turret-rim velocities can then be estimated closely by the following relation:

$$\left(\frac{V}{V_o}\right)_{\text{turret rim}} = \frac{\left(\frac{V}{V_o}\right)_{\text{oblate-spheroid rim}}}{\left(\frac{V}{V_o}\right)_{\text{oblate-spheroid top}}} \left(\frac{V}{V_o}\right)_{\text{turret top}}$$

Wing interference velocities at $\alpha = 1^\circ$ were added to the estimated turret-rim velocities and the resulting total velocities were converted to low-speed pressure coefficients by equation (3). Compressibility effects were accounted for by the procedure used in the estimations for the chordwise central meridian. The pressure estimates for the rim of the forward portion of the upper turret at $\alpha = 1^\circ$ are given in figure 13. Measured rim pressures are shown for comparison.

The rim pressures over the rearward portion of the turret could not be calculated. Experimental data (reference 6) indicate, however, that for such bodies the pressures are nearly constant across the span at corresponding distances behind the maximum thickness. The pressure coefficients for the rim of the rearward portion of the turret were therefore assumed to be the same as those along the chordwise central meridian (fig. 9(a)) and are shown in figure 13.

Spanwise at maximum thickness (line 3, fig. 3).- It has already been shown that the forward portion of the turret can be approximated by an oblate spheroid. (See fig. 11.)

[redacted]

For an oblate spheroid, the velocity over the central meridian normal to the flow is equal to the constant L of equation (7). From this consideration, the velocity over the spanwise section of the turret at maximum thickness is assumed to be constant and equal to the value previously calculated at maximum thickness on line 1.

## ESTIMATION OF PRESSURES OVER WING SURFACE NEAR TURRET

Velocity decay.- In the determination of loads over the wing surface surrounding the turret, the turret was considered to be adding interference velocities to the velocities for the wing alone. Calculations were made along lines extended over the wing surface chordwise in front of the turret (line 1 extended) and spanwise from the side of the turret (line 3 extended) as shown in figure 3.

The forward portion of the upper turret was represented by the same oblate spheroid used in previous calculations (see fig. 11) and velocity ratios were calculated for this shape by equation (5) with $\zeta \geq \zeta_o$. Along line 3 extended spanwise, $\mu = 0$ and $\omega = \frac{\pi}{2}$; along line 1 extended chordwise, $\mu = \omega = 0$. The calculated velocity ratio $V/V_o$ was expressed as the velocity-increment ratio $\Delta V/V_o$ by the relation given in equation (2), and the decay ratio $\Delta V/(\Delta V)_{max}$ or $\Delta V/(\Delta V)_{min}$ was expressed as the ratio of $\Delta V/V_o$ for $\zeta \geq \zeta_o$ to $\Delta V/V_o$ for $\zeta = \zeta_o$.

The decay ratio with incompressible flow was calculated as a function of $\zeta$ and expressed in terms of distance $r_i$ from the turret surface as

$$r_i = a\left(\frac{\sqrt{\zeta^2 + 1}}{\sqrt{\zeta_o^2 + 1}} - 1\right) \qquad (9)$$

where a is the length of the semimajor axis. The expansion of the field for compressibility was taken

into account by plotting $\Delta V/(\Delta V)_{max}$ against r instead of $r_i$ where, from reference 7,

$$r = \frac{r_i}{\sqrt{1 - M^2}} \tag{10}$$

Figure 14 shows the velocity decay ratios calculated for the oblate spheroid and compared with the values derived from measurements on the wing near the surface of the turret. The theory of the expansion of the field (equation (10)) given in reference 7 is not developed for the chordwise direction. The experimental values shown in figure 14 were obtained by deducting the velocities over the wing alone from the velocities obtained at corresponding points on the wing with the turret added.

Spanwise loads (line 3 extended).- In the determination of the estimated spanwise loads, the first step was the determination of the velocity ratio for the wing alone $(V/V_o)_w$. Velocity-increment ratios, previously calculated for incompressible flow, were obtained from figure 5 for the wing alone at angles of attack of $1^\circ$ and $4^\circ$. These velocity-increment ratios for the wing were converted to low-speed pressure coefficients by the use of equations (2) and (3) and these values were adjusted for compressibility by the von Kármán relation (equation (4)). The corresponding velocity ratios $(V/V_o)_w$ were obtained from the relation

$$\left(\frac{V}{V_o}\right)^2 = 1 - \frac{2}{(\gamma - 1)M^2}\left[\left(1 + \frac{\gamma}{2}PM^2\right)^{\frac{\gamma-1}{\gamma}} - 1\right] \tag{11a}$$

The velocity ratio for the turret with wing interference $(V/V_o)_{max}$ was determined by use of equation (11a) from the estimated pressure coefficients over the turret chordwise central meridian (line 1) at maximum thickness as shown in figures 9 and 10.

The turret interference velocity at the surface of the turret was then defined as

$$\left(\frac{\Delta V}{V_o}\right)_{max} = \left(\frac{V}{V_o}\right)_{max} - \left(\frac{V}{V_o}\right)_w$$

and the turret interference velocity for a point on the wing at a distance from the turret was taken as

$$\left(\frac{\Delta V}{V_o}\right)_t = \frac{\Delta V}{(\Delta V)_{max}}\left(\frac{\Delta V}{V_o}\right)_{max}$$

where $\Delta V/(\Delta V)_{max}$ is the decay ratio.

Total wing velocities including turret interference velocities were given by the relation

$$\frac{V}{V_o} = \left(\frac{V}{V_o}\right)_w + \left(\frac{\Delta V}{V_o}\right)_t$$

Pressure coefficients were obtained from the total velocities by use of the formula

$$P = \frac{2}{\gamma M^2}\left\{1 - \frac{\gamma - 1}{2}M^2\left[\left(\frac{V}{V_o}\right)^2 - 1\right]\right\}^{\frac{\gamma}{\gamma-1}} - \frac{2}{\gamma M^2} \qquad (11b)$$

Figure 15 gives estimated pressure coefficients over the wing surface spanwise from the side and over the top of the upper turret for wing angles of attack of 1° and 4° with Mach numbers of 0.275 and 0.500. Experimental values are given for comparison.

Chordwise loads (line 1 extended).- For spanwise loads, $(V/V_o)_w$ was assumed constant because all calculations were made for the same chordwise location. This assumption could not be applied to chordwise estimations because the wing velocity gradient was significant. It

[redacted]

thus became necessary to obtain $(V/V_o)_w$ for each point considered; otherwise, the procedure was similar to that for the spanwise loads.

The assumption of a stagnation point gave a negative turret interference velocity at the surface (turret leading edge)

$$\left(\frac{\Delta V}{V_o}\right)_{min} = -\left(\frac{V}{V_o}\right)_w$$

where $(V/V_o)_w$ was the velocity ratio for the wing alone at the location of the turret leading edge.

Values of $(\Delta V/V_o)_t$, $V/V_o$, and $P$ were then estimated as for the spanwise loads but with the use of the chordwise decay ratio given in figure 14(b) and with minimum values substituted for maximum.

The estimated and experimental pressure coefficients over the wing surface chordwise in front of the upper turret for wing angles of attack of $1^\circ$ and $4^\circ$ and at Mach numbers of 0.275 and 0.500 are given for comparison in figure 16. In the absence of theory concerning the effect of compressibility on the extension of the field, the decay curve for incompressible flow was used.

## DISCUSSION

The generally satisfactory agreement shown in figures 8 to 10 and 13 between the estimated and the experimental pressure distributions may be taken as experimental verification of the validity of the method of accounting for interference by the addition of induced velocities. (This method is of course subject to certain limitations that are pointed out in reference 1.) In addition, the remarkable agreement between the estimated and experimental velocity decay ratios and pressures along two lines extending in front of and from the side of the turret (figs. 14 to 16) provides an excellent check on the potential-flow method of estimating

the pressures surrounding a protuberance. As indicated by the potential theory, the influence of a protuberance on the surrounding pressures decreases very rapidly with distance from the surface.

The effect of compressibility on pressures over the turrets is expressed satisfactorily up to the critical Mach number by the von Kármán relation (equation (4)). (See figs. 7 to 10 and 13.) At Mach numbers much higher than the critical, however, the von Kármán relation fails completely to describe the changes that occur. As shown in figure 10, the negative pressure coefficients at supercritical speeds may either exceed or fail to reach the estimated values. Additional study is needed before the pressure loads at supercritical speeds can be predicted with confidence.

The assumption concerning expansion with Mach number of the field normal to the turret (equation (10)) is not quantitatively checked because the experimental data are of insufficient accuracy; from figure 14(a), however, this assumption appears to be at least qualitatively correct and the extent of the velocity field outward appears to increase at least as much as is given by equation (10). It also appears from the experimental data (fig. 14(b)) that the assumption of some expansion of the field with Mach number chordwise in front of the turret would bring the estimation into closer agreement with experiment but this condition should not be taken as proof that such expansion occurs.

Although within the range of applicability of the method (subcritical speeds) the peak negative pressures and consequently the critical speeds have been predicted with considerable accuracy as may be seen from figure 7, some divergences appear in other parts of the estimations. The disparity that exists between estimated and experimental values in the subcritical range is due largely to inaccuracy in calculating the velocities over the turrets alone. The divergences for the subcritical Mach number range shown in figures 8 to 10, for instance, may be explained to a great extent by the fact that the slope method used in the estimations is most accurate in regions of small slope, as at the maximum thickness of the turret, and least accurate where the slope is large, as at the front and rear. For the estimations of figure 15, constant pressure spanwise across the surface of the turret was assumed as for the case of the oblate

[redacted]

spheroid, whereas the actual negative pressure coefficients are larger at the center. The agreement between estimated and experimental spanwise decay ratios shown in figure 14(a) indicates that the departure of the shape of the rearward portion of the turret from that of the oblate spheroid apparently has very little effect on the spanwise decay of velocities. The underestimation of pressures over the wing surface spanwise from the side of the turret (fig. 15) is accounted for by a slight underestimation of $(\Delta V/V_o)_{max}$. The estimated and measured pressures chordwise in front of the turret agree well although the measured values do not appear altogether consistent.

The general methods employed in the present investigation may be expected to apply with accuracy sufficient for design purposes not only to estimations for similar shapes but also to estimations for shapes varying considerably from the shapes considered herein. Assumptions made in connection with the methods, however, should be in keeping with the suggestions outlined in reference 1; for instance, the assumption of an empirical correction factor for reducing calculated two-dimensional velocities to three-dimensional velocities may be expected to apply to shapes other than those considered herein if the ratio of three-dimensional to two-dimensional velocities can be determined for similar bodies. A discussion of this assumption is given in reference 1. The relation assumed between top and rim velocities for the turrets in the present report may also be expected to apply with reasonable accuracy to other bodies that can be represented by simple geometrical shapes, such as oblate or prolate spheroids, over which the velocities are calculable. The assumption of approximately constant velocities spanwise across the rear portion of the turrets has been verified experimentally in reference 6 for other shapes considerably different from those considered in the present investigation.

## CONCLUSIONS

The applicability of current methods of estimating pressures over and near protuberances to turrets located

on a wing in regions of high interference velocities was investigated. A comparison of estimated and measured data resulted in the following conclusions:

1. Current methods of estimating pressures over protuberances were verified.

2. Methods of predicting the influence of a protuberance on pressures over the surrounding surface were found to be accurate.

3. The accuracy of estimations was sufficient for design purposes and for predicting the critical speeds of the turrets.

4. The methods used in this paper were not applicable to estimations at speeds much higher than the critical.

Langley Memorial Aeronautical Laboratory
National Advisory Committee for Aeronautics
Langley Field, Va.

[redacted]

## REFERENCES

1. Wright, Ray H.: Estimation of Pressures on Cockpit Canopies, Gun Turrets, Blisters, and Similar Protuberances. NACA ACR No. L4E10, 1944.

2. Mattson, Axel T.: Tests of a Large Spherical Turret and a Modified Turret on a Typical Bomber Fuselage. NACA ARR, Oct. 1942.

3. Theodorsen, Theodore: Theory of Wing Sections of Arbitrary Shape. NACA Rep. No. 411, 1931.

4. von Kármán, Th.: Compressibility Effects in Aerodynamics. Jour. Aero. Sci., vol. 8, no. 9, July 1941, pp. 337-356.

5. Munk, Max M.: Fluid Mechanics, Pt. II. Ellipsoids of Revolution. Vol. I of Aerodynamic Theory, div. C, ch. VII, sec. 11, W. F. Durand, ed., Julius Springer (Berlin), 1934, pp. 289-292.

6. Delano, James B., and Wright, Ray H.: Investigation of Drag and Pressure Distribution of Windshields at High Speeds. NACA ARR, Jan. 1942.

7. Prandtl, L.: General Considerations on the Flow of Compressible Fluids. NACA TM No. 805, 1936.

[redacted]

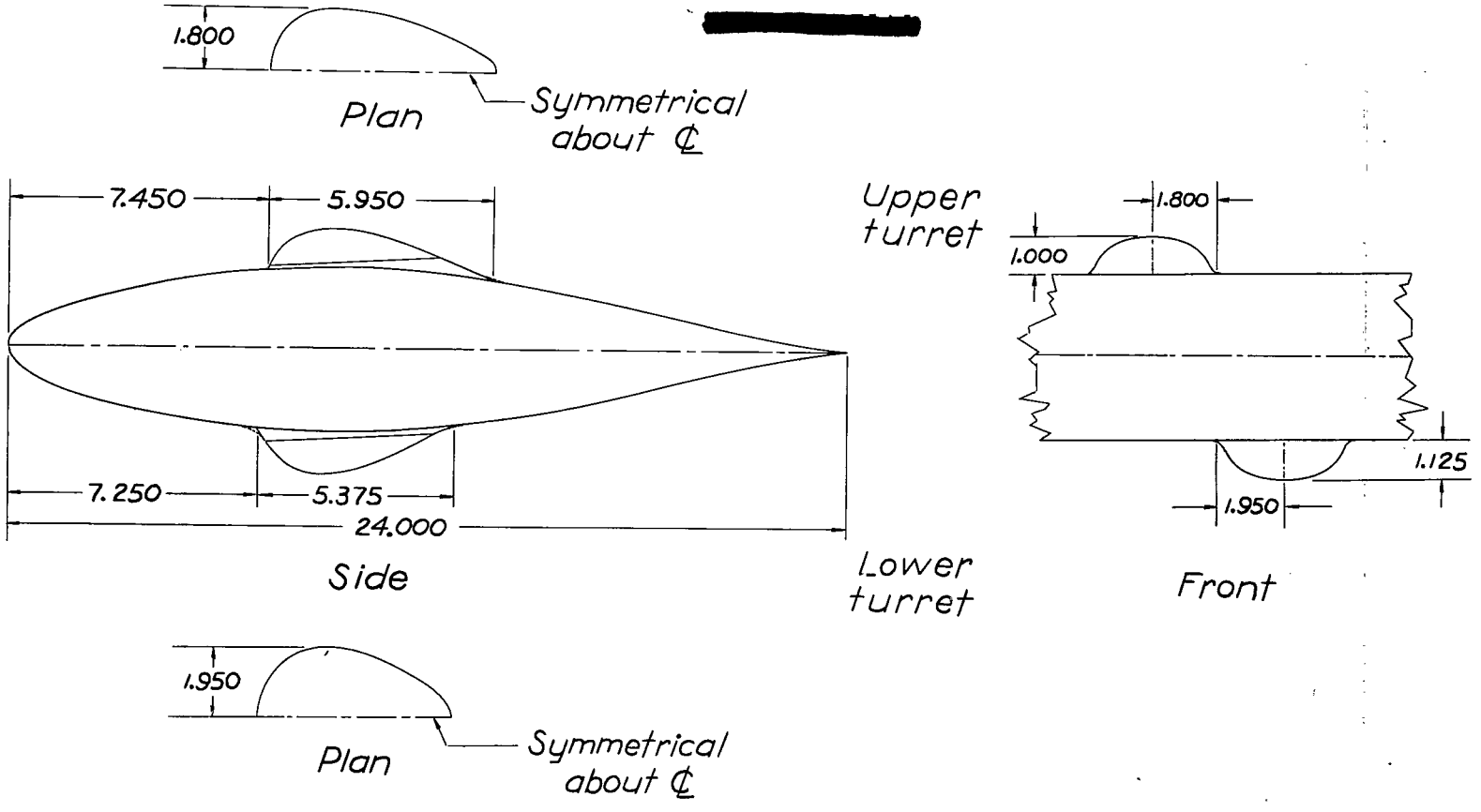


NATIONAL ADVISORY COMMITTEE FOR AERONAUTICS

Figure 1.- General details of the turrets mounted on a symmetrical wing section. All dimensions are given in inches.

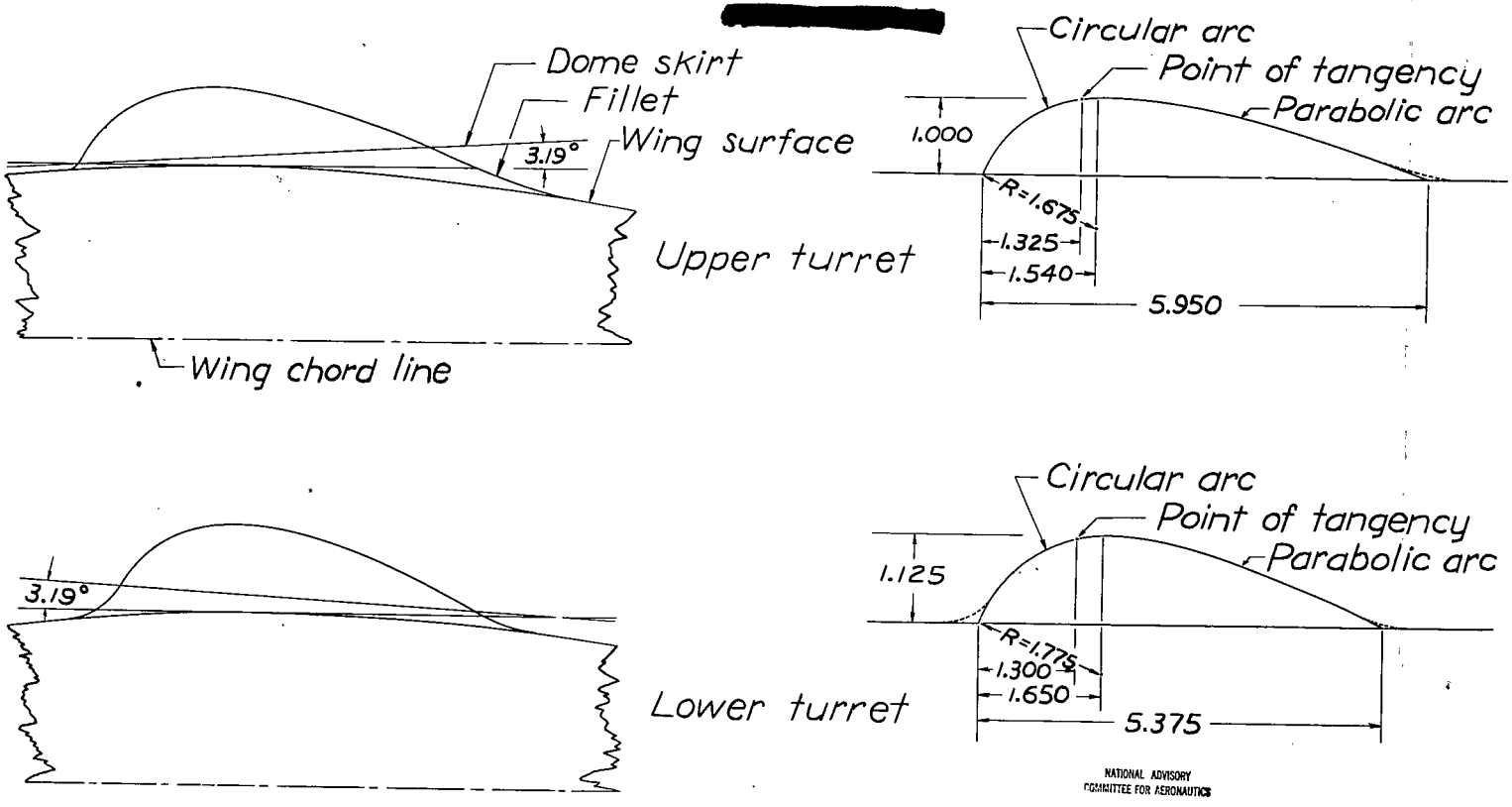


(a) Actual shapes of the turrets as installed on the wing.

(b) Effective shapes of the turrets with wing surface reduced to a straight line.

Figure 2.- Actual and effective turret-profile shapes. All dimensions are given in inches.

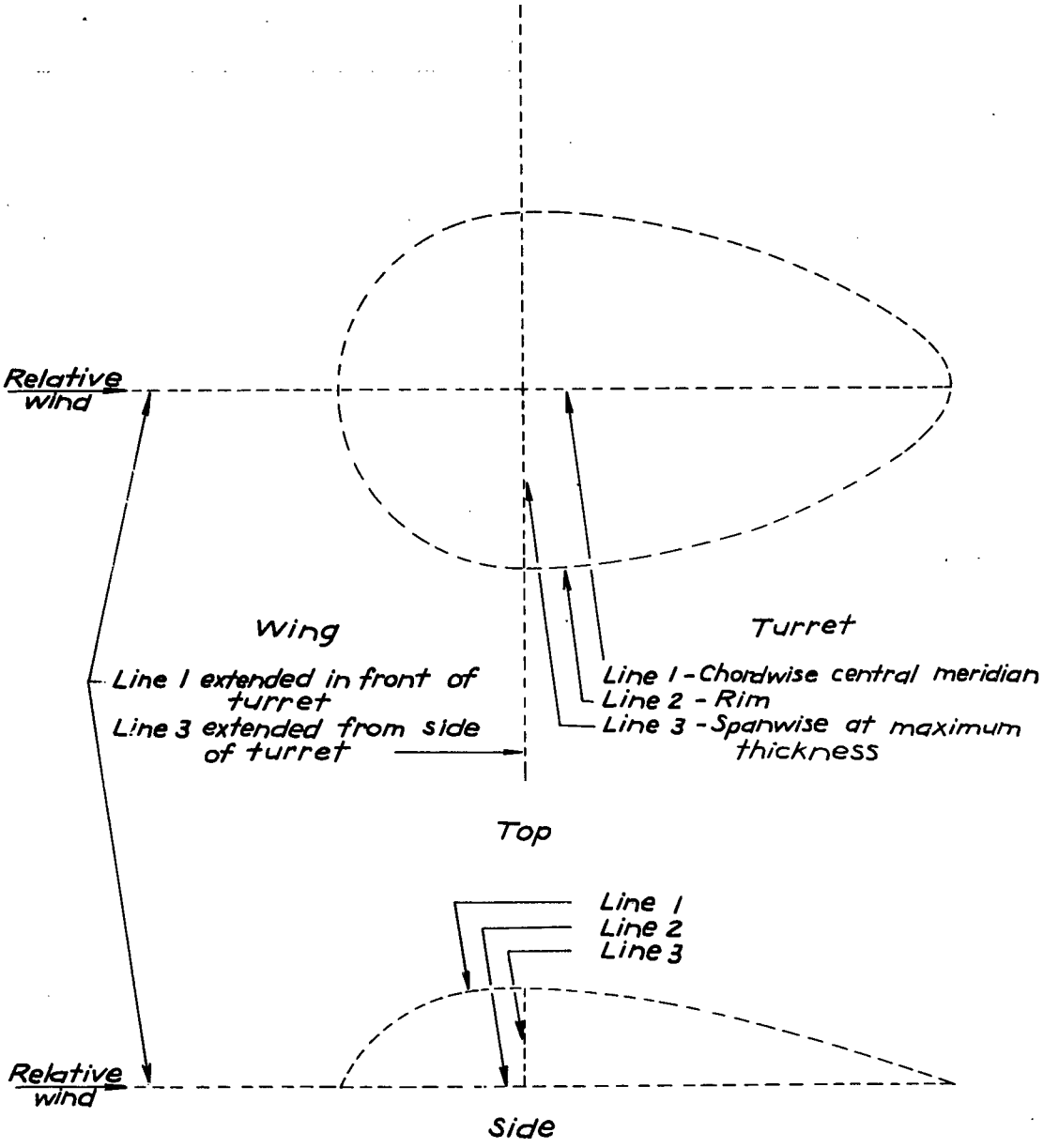


NATIONAL ADVISORY
COMMITTEE FOR AERONAUTICS

Figure 3.- Regions of pressure estimations over turret and surrounding wing surface.

[redacted]

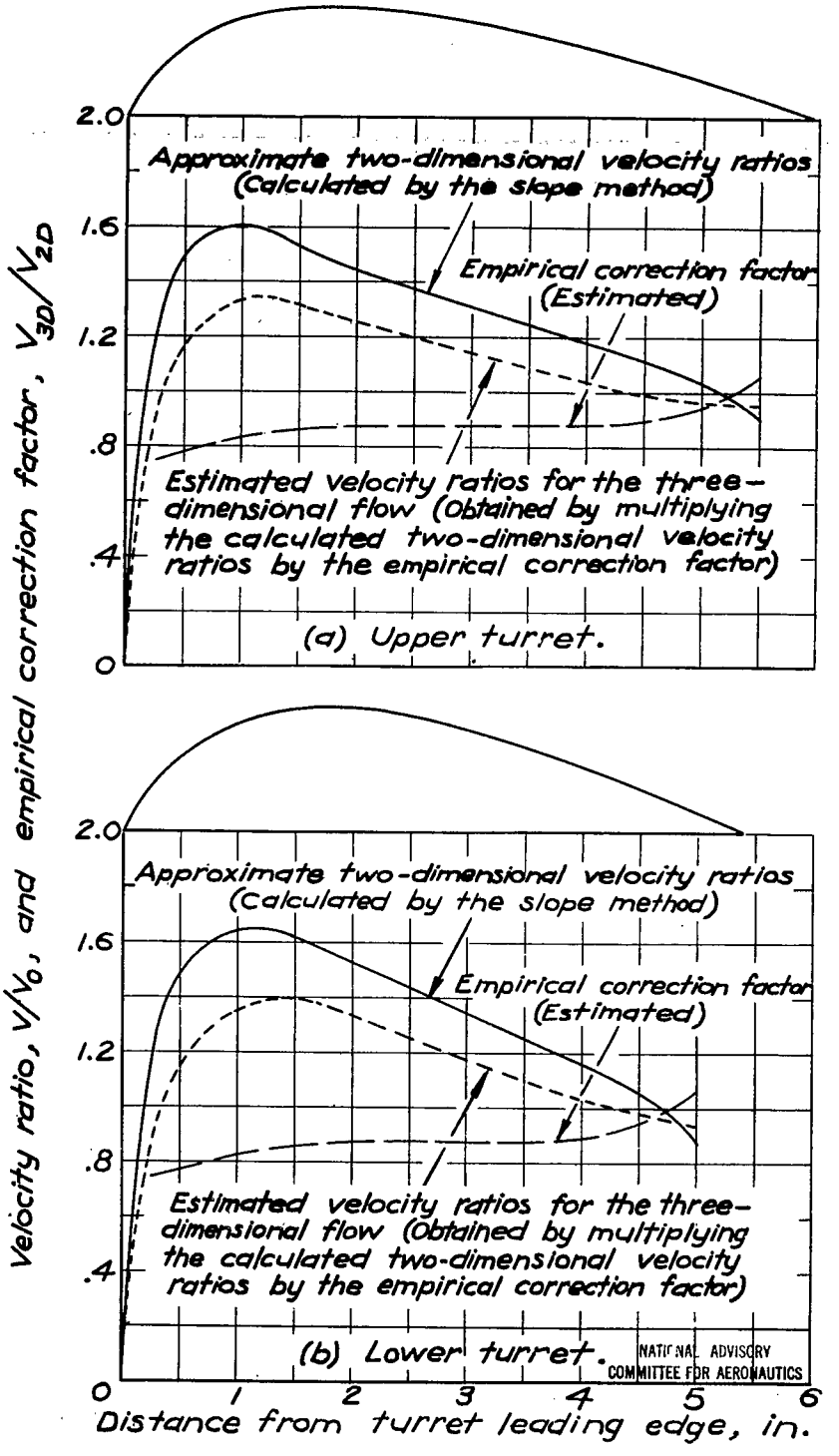


Figure 4.- Estimated velocities for the chordwise central meridian of the turrets without wing interference. $M = 0$.

[redacted]

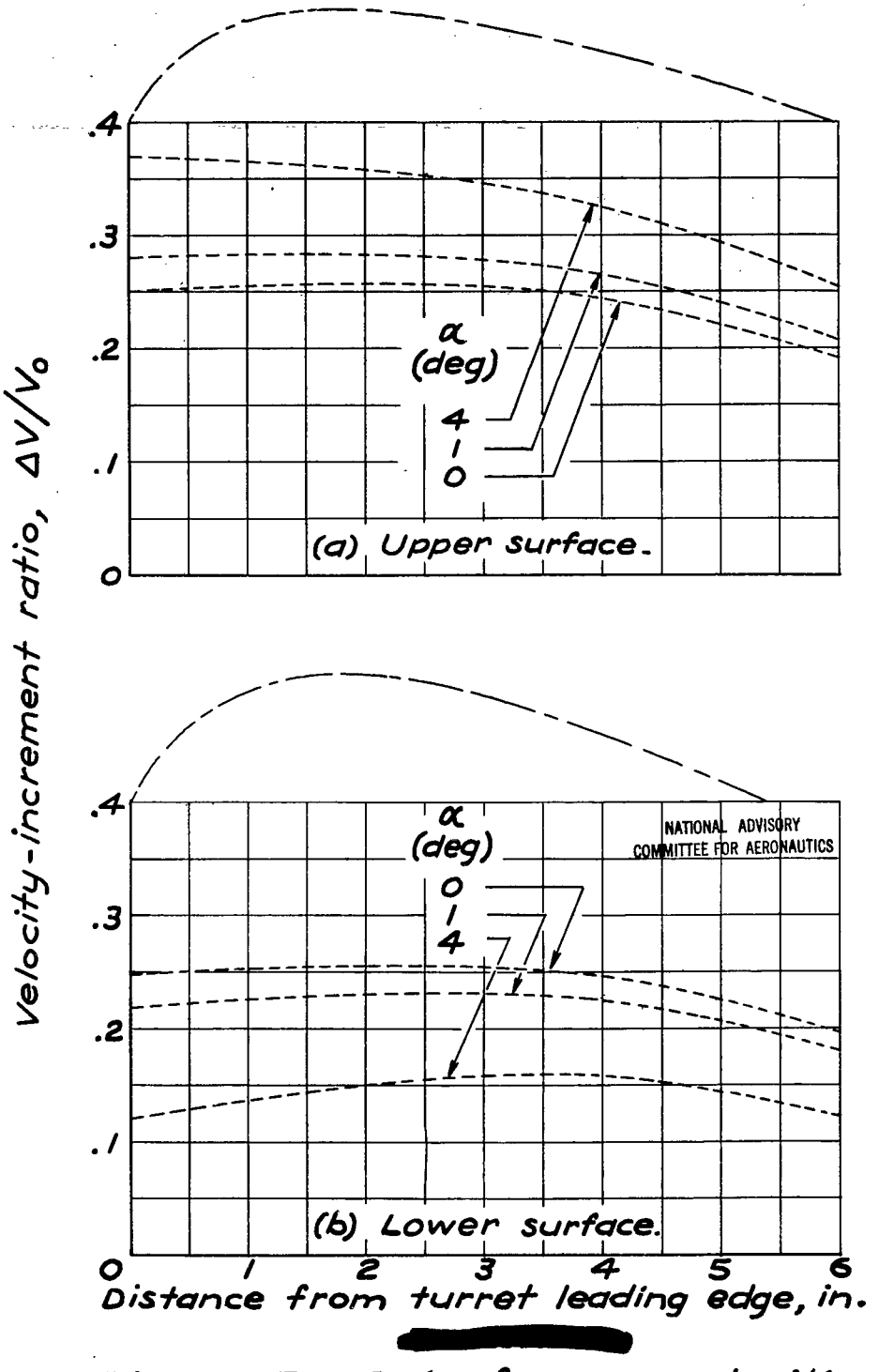


[redacted]

Figure 5.- Interference velocities calculated for the wing alone. M = 0.

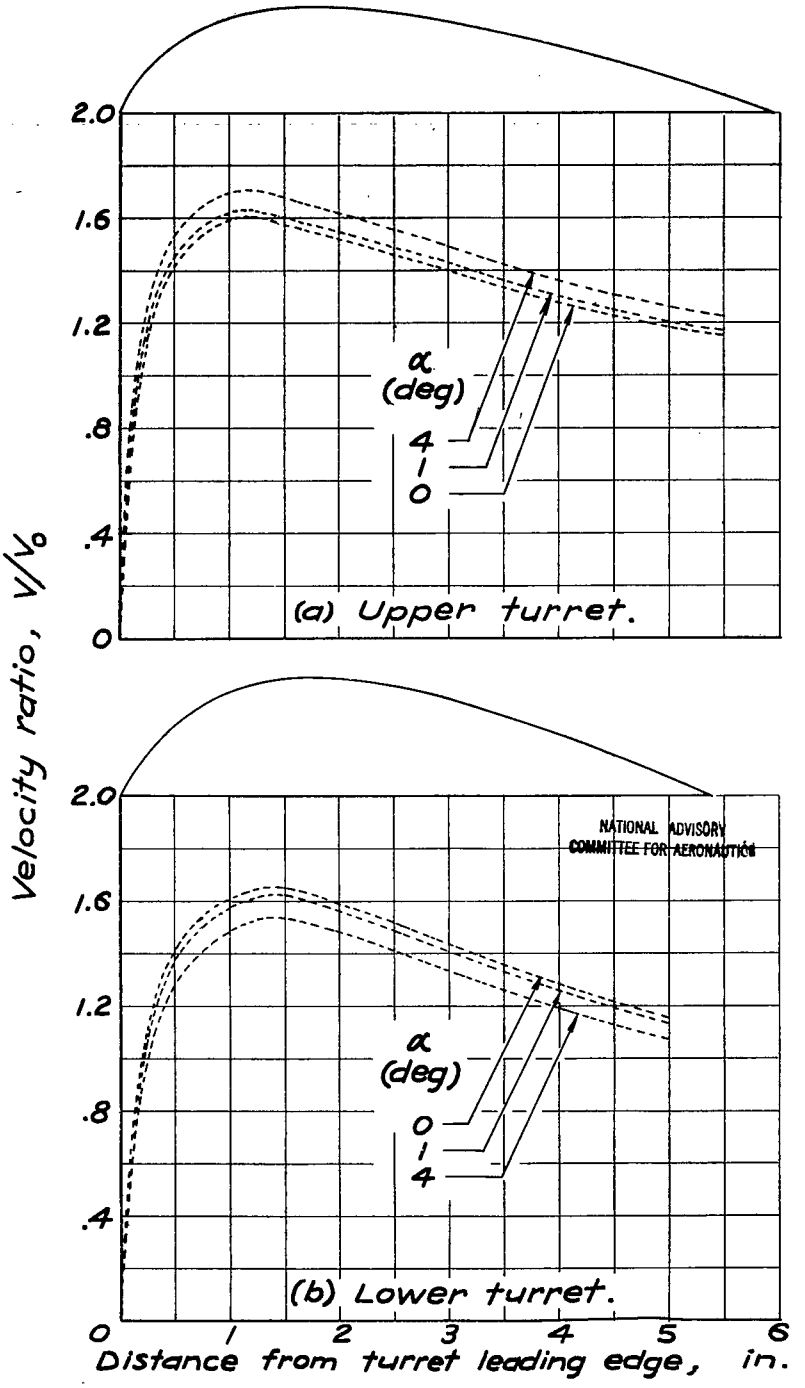


Figure 6.- Estimated velocities for the chordwise central meridian of the turrets with wing interference. M = 0.

[redacted]

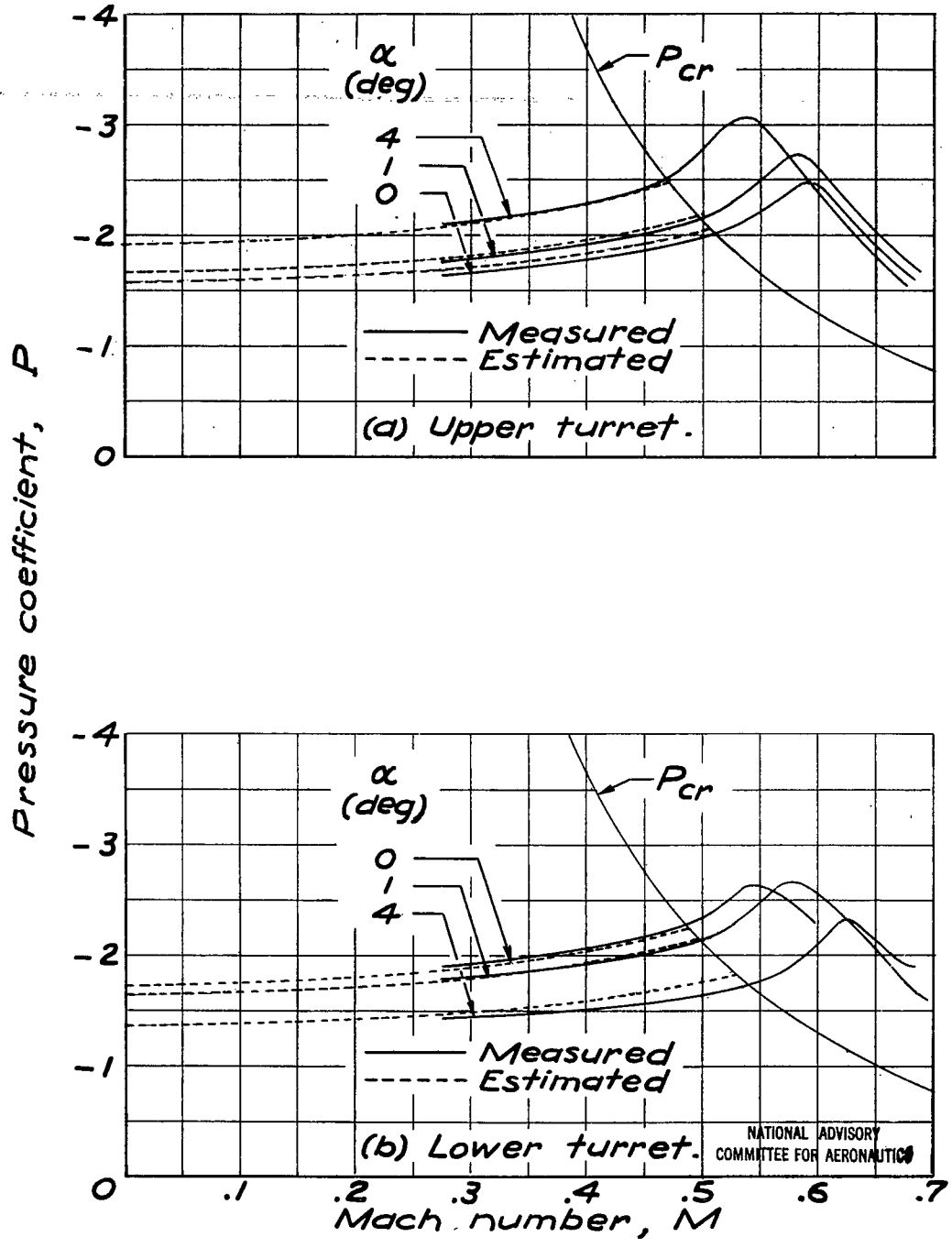


Figure 7.- Variation of peak negative pressure coefficients with Mach number for the chordwise central meridian of the turrets with wing interference.

[redacted]

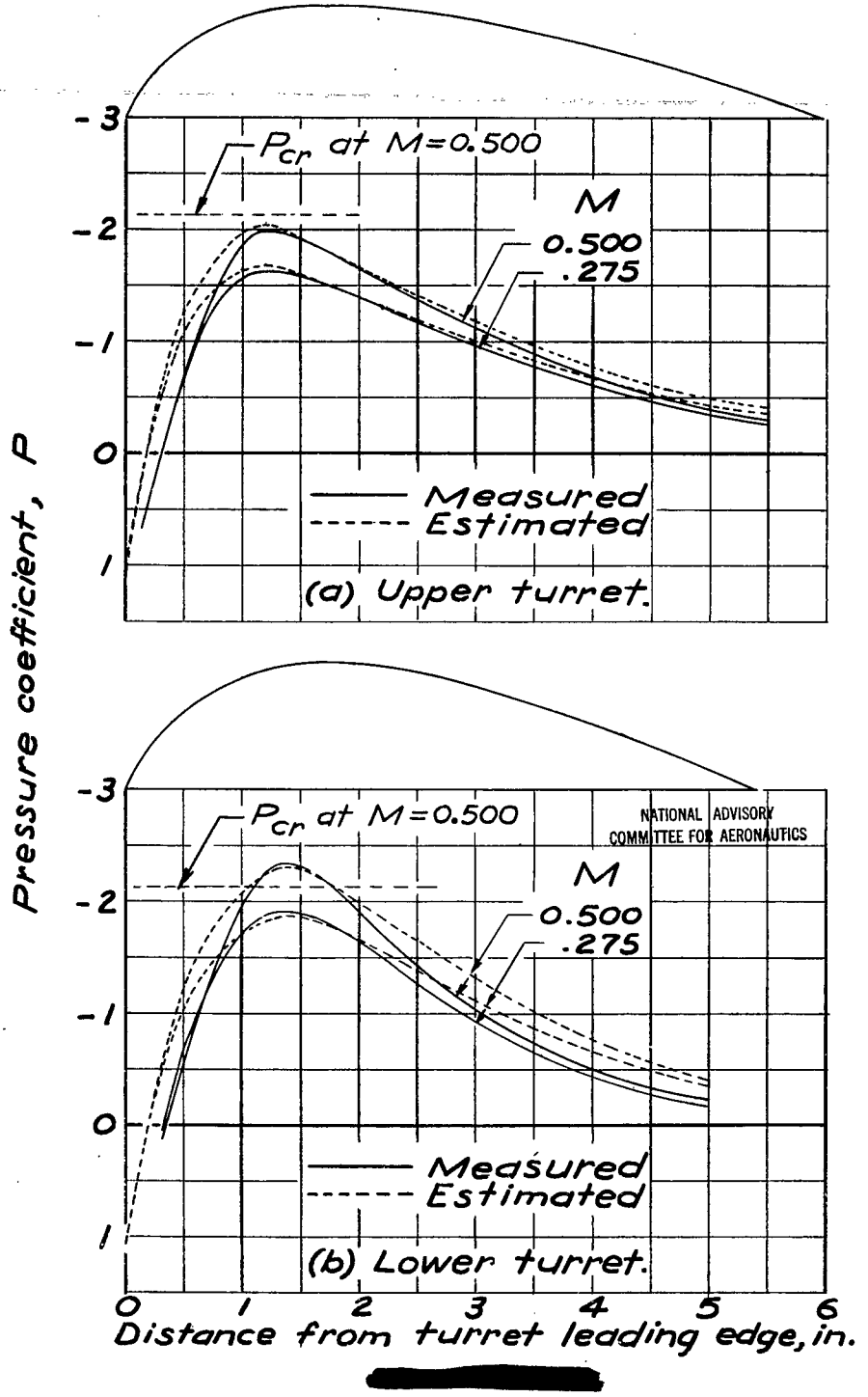


[redacted]

Figure 8.- Pressure distributions for the chordwise central meridian of the turrets with wing interference. $\alpha = 0°$.

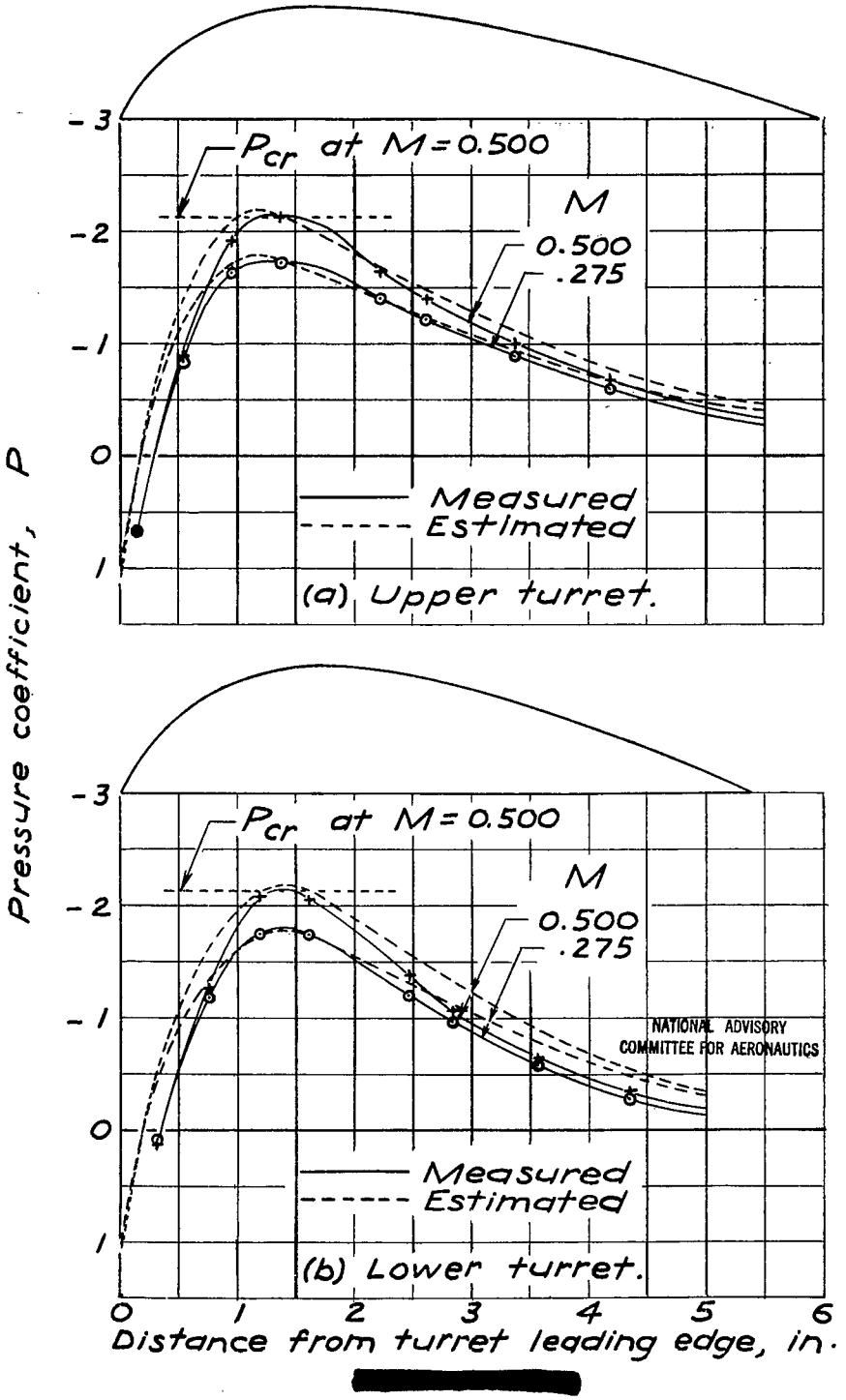


[redacted]

Figure 9.- Pressure distributions for the chordwise central meridian of the turrets with wing interference. $\alpha = 1°$.

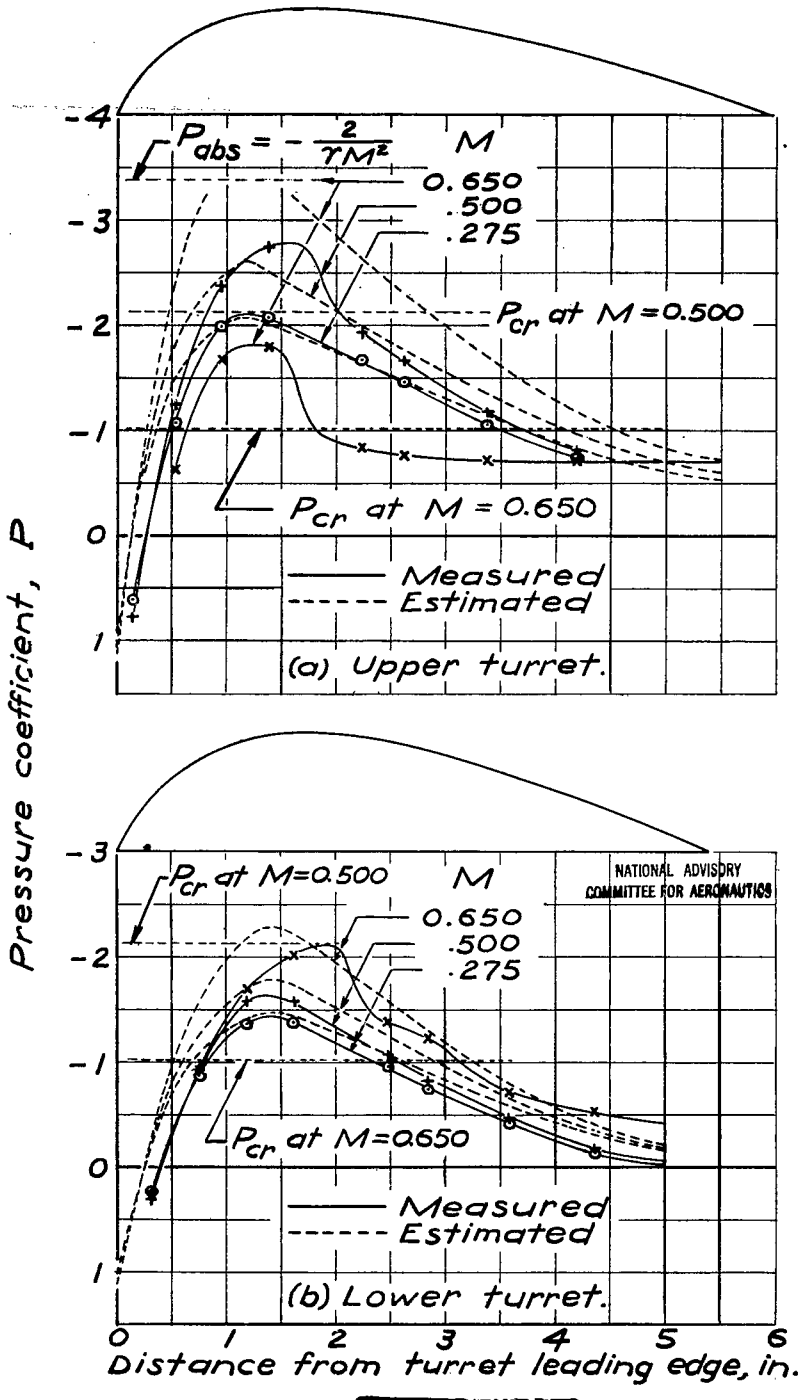


[redacted]

Figure 10.- Pressure distributions for the chordwise central meridian of the turrets with wing interference. $\alpha = 4°$.

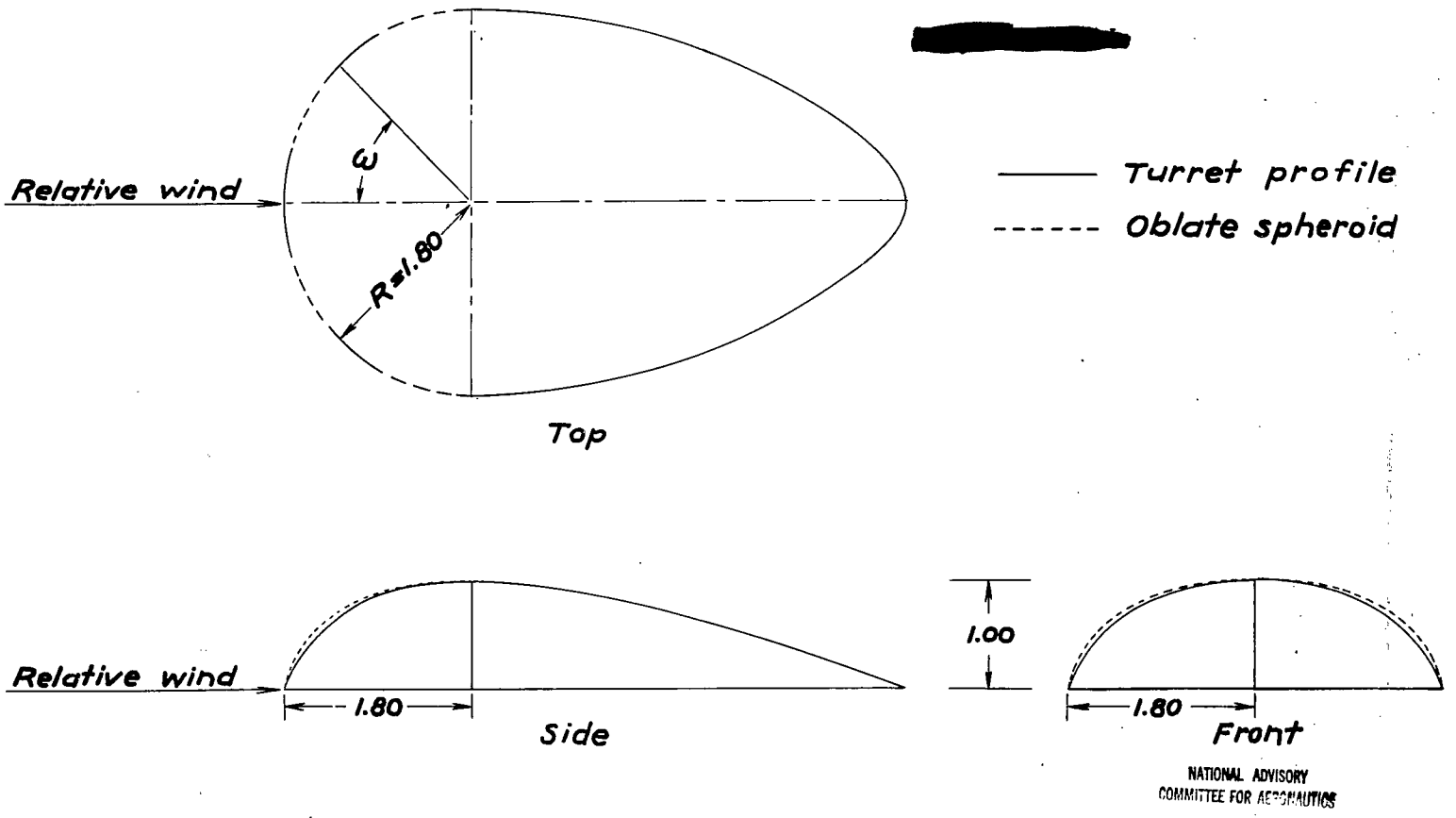


Figure 11.- The forward portion of the upper turret represented by an oblate spheroid. All dimensions are given in inches.

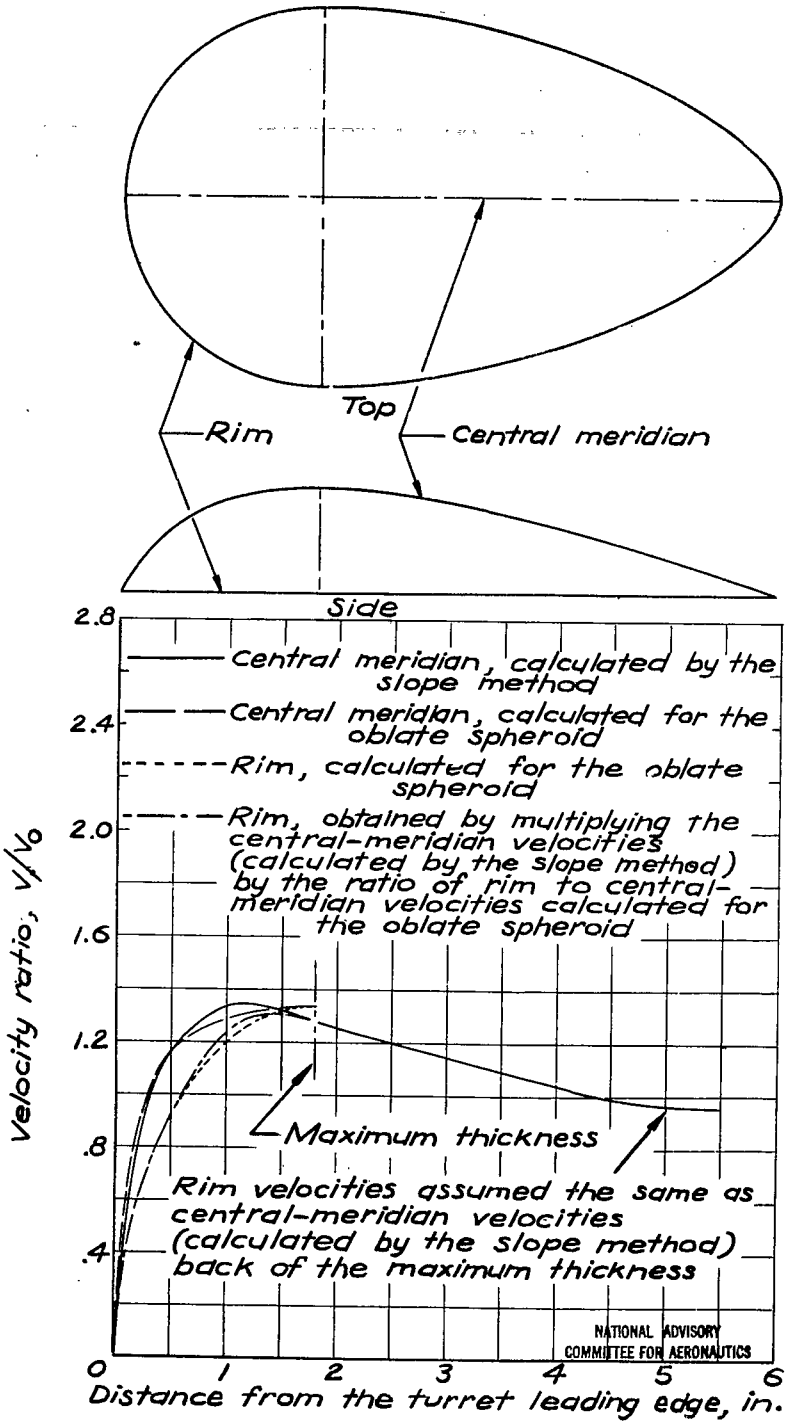


Figure 12.- Estimated velocities around the rim of the upper turret without wing interference. $M = 0$.

[redacted]

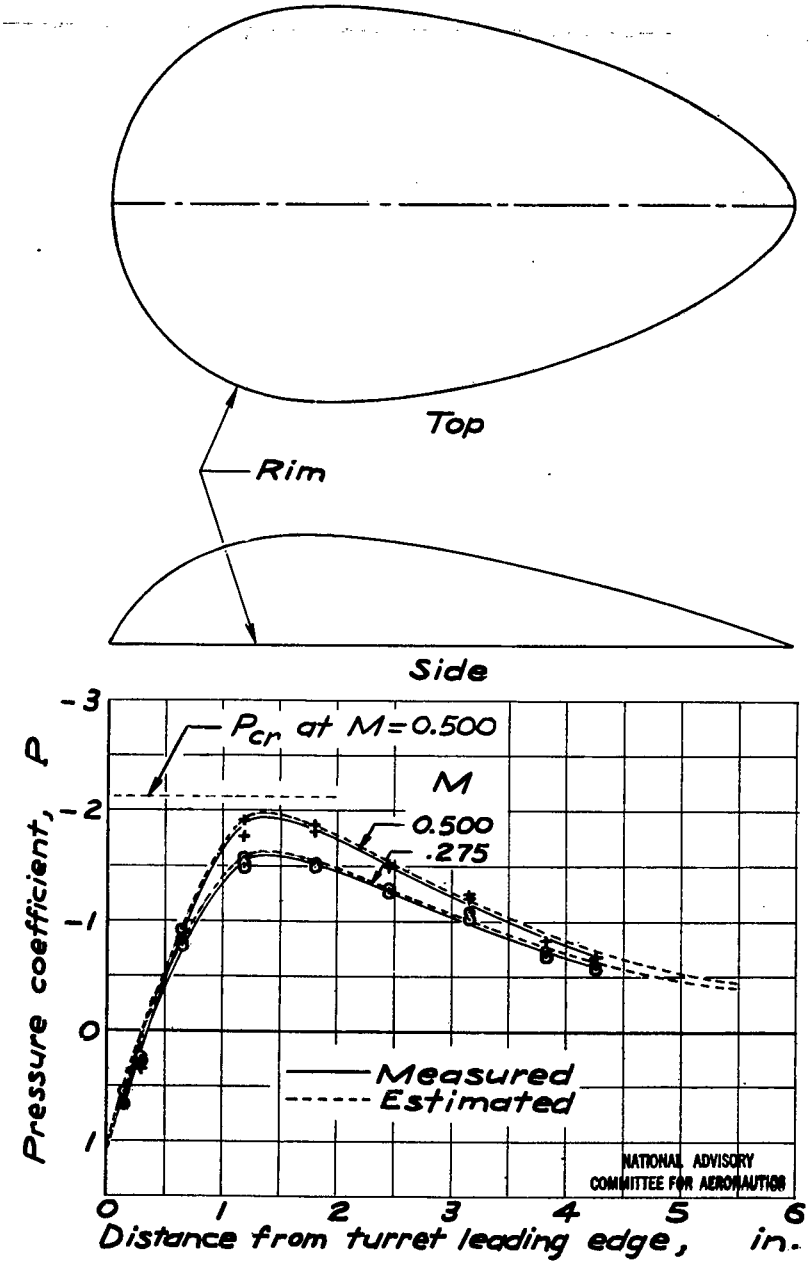


Figure 13.- Pressure distributions for the rim of the upper turret with wing interference. $\alpha = 1°$.

[redacted]

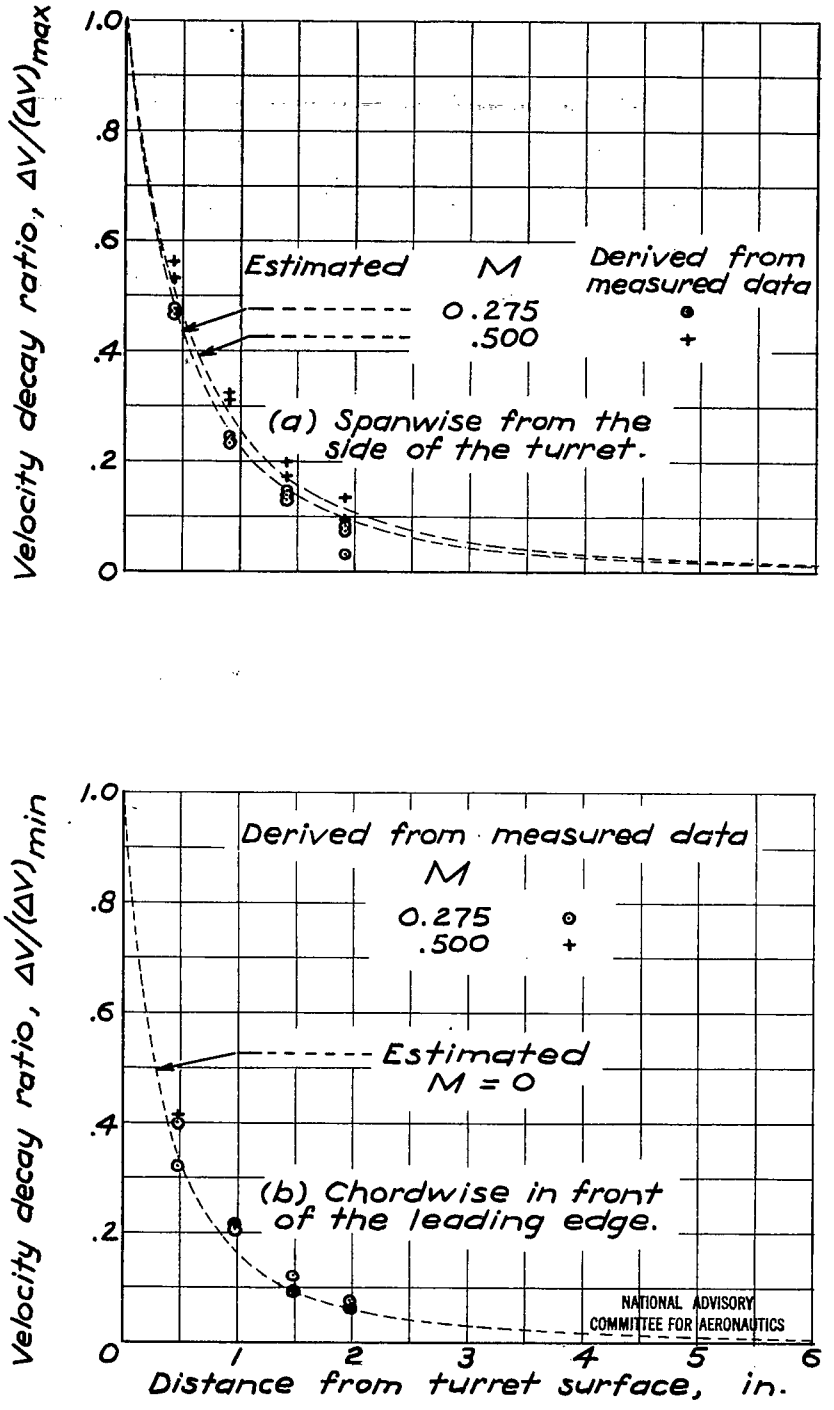


Figure 14.- Velocity decay with distance from the turret surface.

[redacted]

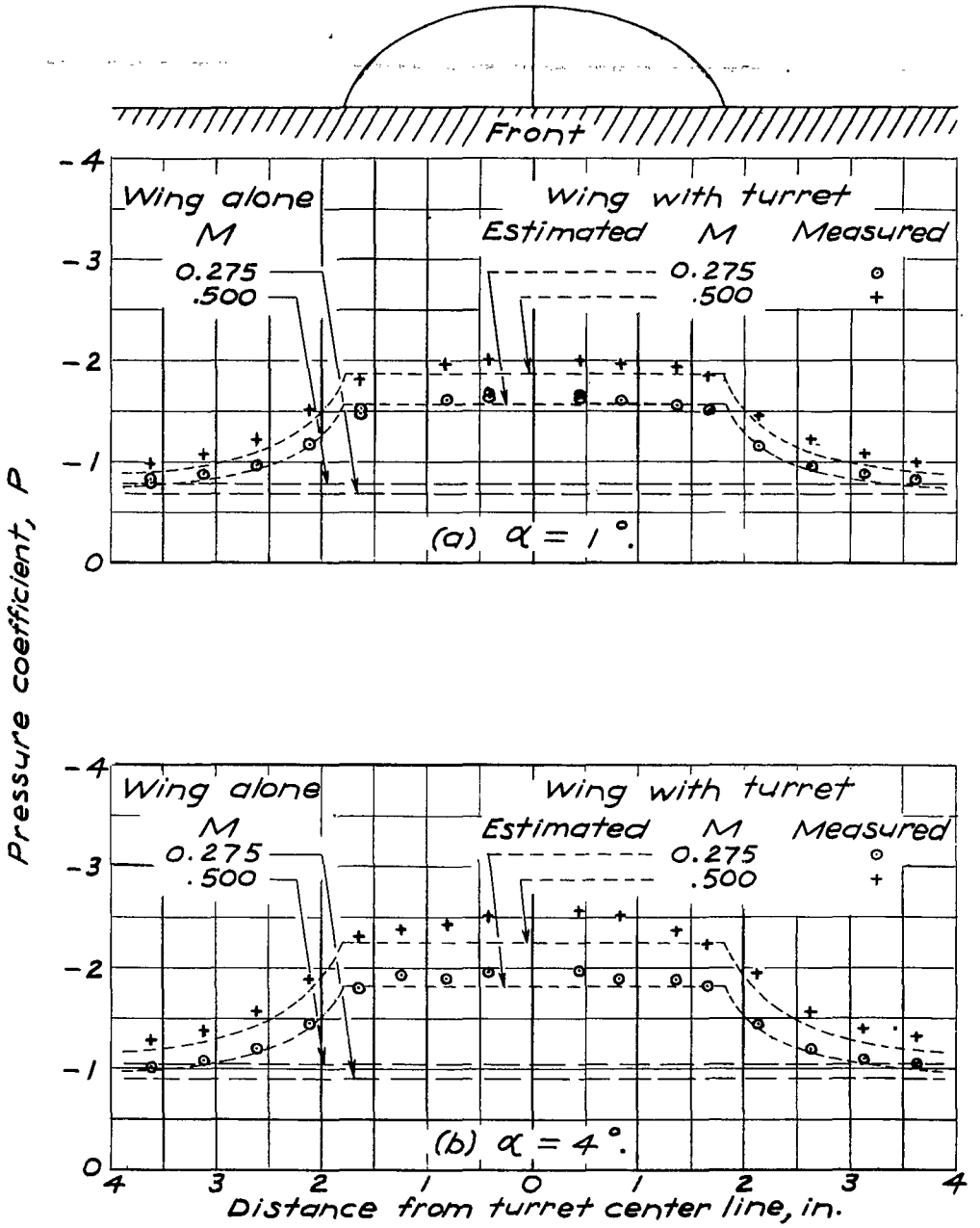


NATIONAL ADVISORY COMMITTEE FOR AERONAUTICS

Figure 15.- Pressure distributions spanwise over the upper turret at maximum thickness and over the wing surface near the turret.

[redacted]

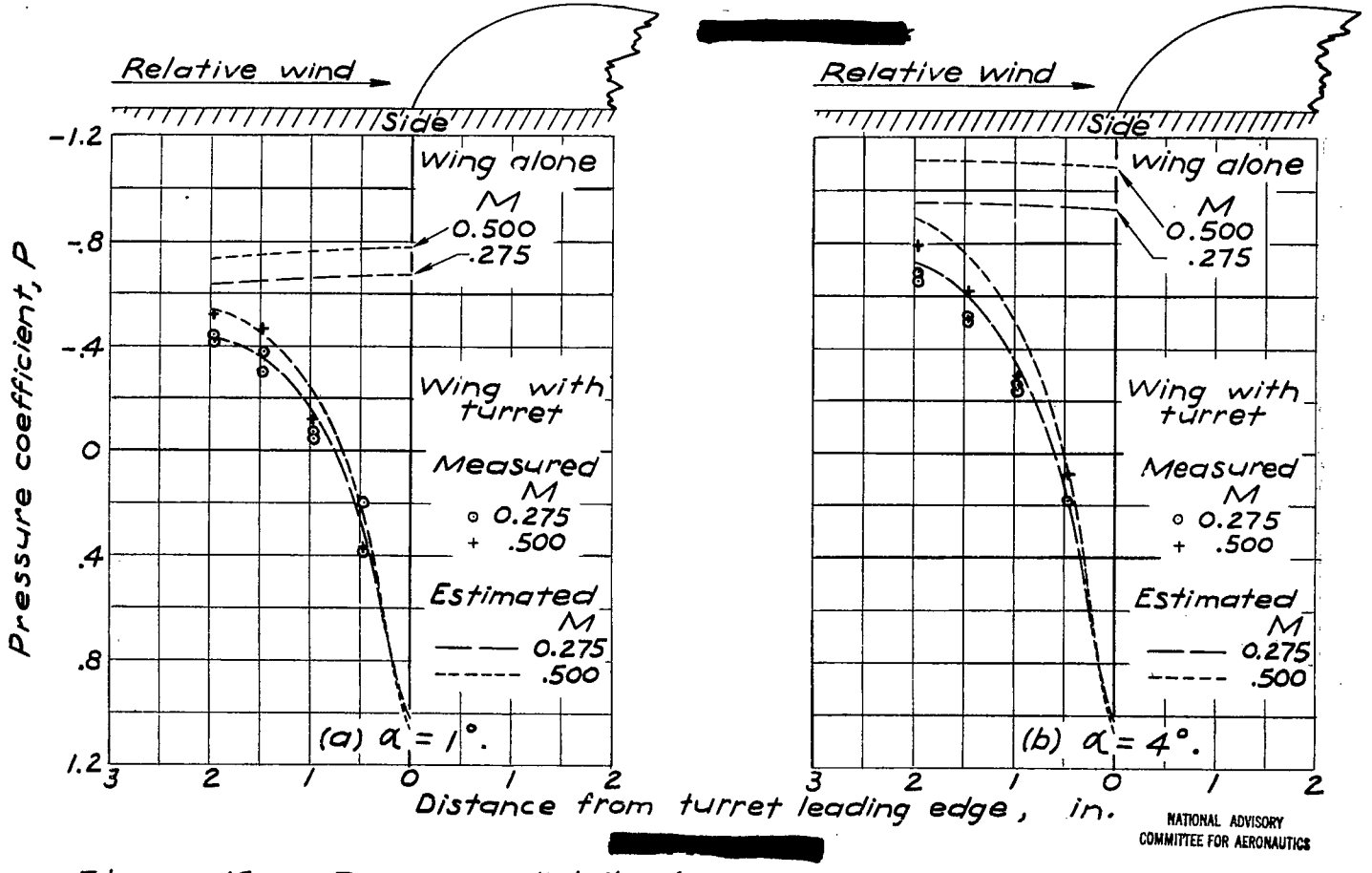


Figure 16.- Pressure distributions chordwise over the wing surface in front of the upper turret.

NASA Technical Library
3 1176 01403 3741